

Low-Dose Perampanel Rescues Cortical Gamma Dysregulation Associated With Parvalbumin Interneuron GluA2 Upregulation in Epileptic *Syngap1*^{+/−} Mice

Brennan J. Sullivan, Simon Ammanuel, Pavel A. Kipnis, Yoichi Araki, Richard L. Huganir, and Shilpa D. Kadam

ABSTRACT

BACKGROUND: Loss-of-function *SYNGAP1* mutations cause a neurodevelopmental disorder characterized by intellectual disability and epilepsy. *SYNGAP1* is a Ras GTPase-activating protein that underlies the formation and experience-dependent regulation of postsynaptic densities. The mechanisms that contribute to this proposed monogenic cause of intellectual disability and epilepsy remain unresolved.

METHODS: We established the phenotype of the epileptogenesis in a *Syngap1*^{+/−} mouse model using 24-hour video electroencephalography (vEEG)/electromyography recordings at advancing ages. We administered an acute low dose of perampanel, a Food and Drug Administration-approved AMPA receptor (AMPAR) antagonist, during a follow-on 24-hour vEEG to investigate the role of AMPARs in *Syngap1* haploinsufficiency. Immunohistochemistry was performed to determine the region- and location-specific differences in the expression of the GluA2 AMPAR subunit.

RESULTS: A progressive worsening of the epilepsy with emergence of multiple seizure phenotypes, interictal spike frequency, sleep dysfunction, and hyperactivity was identified in *Syngap1*^{+/−} mice. Interictal spikes emerged predominantly during non-rapid eye movement sleep in 24-hour vEEG of *Syngap1*^{+/−} mice. Myoclonic seizures occurred at behavioral-state transitions both in *Syngap1*^{+/−} mice and during an overnight EEG from a child with *SYNGAP1* haploinsufficiency. In *Syngap1*^{+/−} mice, EEG spectral power analyses identified a significant loss of gamma power modulation during behavioral-state transitions. A significant region-specific increase of GluA2 AMPAR subunit expression in the somas of parvalbumin-positive interneurons was identified.

CONCLUSIONS: Acute dosing with perampanel significantly rescued behavioral state-dependent cortical gamma homeostasis, identifying a novel mechanism implicating Ca^{2+} -impermeable AMPARs on parvalbumin-positive interneurons underlying circuit dysfunction in *SYNGAP1* haploinsufficiency.

Keywords: Gamma oscillations, GluA2, Intellectual disability, Myoclonic seizures, Parvalbumin interneurons, Perampanel

<https://doi.org/10.1016/j.biopsych.2019.12.025>

SYNGAP1 codes for synaptic Ras GTPase-activating protein 1 (*SYNGAP1*), a protein critical for the formation of postsynaptic densities and the experience-dependent AMPAR insertion that underlies synaptic plasticity (1–5). Mutations in *SYNGAP1* are prevalent in patients with schizophrenia, intellectual disability (ID), and autism spectrum disorder (6–8). Loss-of-function *SYNGAP1* mutations result in haploinsufficiency and cause mental retardation type 5 (MRD5; Online Mendelian Inheritance in Man #612621), a severe distinct generalized developmental and epileptic encephalopathy with ID, ataxia, severe behavioral problems, and a risk for autism (6–12).

The majority of patients with MRD5 have refractory epilepsy (12). Poor-quality sleep is highly prevalent in patients with

neurodevelopmental disorders (NDDs) and epilepsy (13,14). The relationship between epilepsy and sleep is a major focus of ongoing clinical and preclinical research (13–15). For example, Rett syndrome is an NDD with epilepsy and sleep dysfunction (16,17). Research in both preclinical models of Rett syndrome and patients with Rett syndrome has identified translatable quantitative EEG (qEEG) biomarkers (17,18). There is an urgent need to develop robust biomarkers for NDDs, because bench-to-bedside therapeutic strategies are severely hindered without validated quantitative outcome measures.

Patients with MRD5 predominantly present with myoclonic, absence, or tonic-clonic seizures (8,12). Children with epileptic

SEE VIDEO CONTENT ONLINE

encephalopathies have a slow developmental regression that is primarily due to seizures, interictal spikes (IISs), or cortical dysrhythmia identified on EEG (19,20). Case reports indicate that adult patients demonstrate gradual decline in cognitive abilities (21). Perampanel (PMP), an AMPA receptor (AMPAR) antagonist recently approved by the Food and Drug Administration, has shown significant promise for multiple seizure types in idiopathic generalized epilepsies, including absence seizures (22). Its use in infants with epilepsy is in clinical trial (23). However, the role of AMPAR antagonists such as PMP in *SYNGAP1* haploinsufficiency-related seizures and ID is unknown.

Mice with *Syngap1* haploinsufficiency (*Syngap1*^{+/-}) are relevant translational models presenting with learning and memory deficits, abnormal dendritic spine dynamics, cortical hyperexcitability, and precocious unsilencing of thalamocortical synapses during development (24–26). Currently, no studies have investigated the epileptogenesis, sleep, and underlying mechanisms associated with MRD5. An understanding of the mechanisms that promote spontaneous seizures and network dysfunction can help accelerate the discovery of novel therapeutic strategies. For this purpose, a *Syngap1*^{+/-} loss-of-function mouse model (exon 7 and 8 deletions) (26) underwent 24-hour video EEG/electromyography (EMG) recordings at advancing ages (postnatal day [P] 60 to P120). A subsequent 24-hour EEG investigated the effect of low-dose PMP on EEG-identified biomarkers.

METHODS AND MATERIALS

Animals

All animal care and procedures were carried out in accordance with the recommendations in the Guide for Care and Use of Laboratory Animals of the National Institutes of Health. All protocols used in this study were approved by the Committee on the Ethics of Animal Experiments of Johns Hopkins University. In *Syngap1*^{+/-} mice, exons 7 and 8 (C2 domain) were replaced with a neomycin resistance gene in the opposite direction to eliminate all possible splice variants (26). All mice were single-housed at P46 (7 days before electrode implantation surgeries) in polycarbonate cages with food and water provided ad libitum, on a 12-hour light/dark cycle. All efforts were made to minimize animal suffering and the number of animals used.

Surgery and 24-Hour Video EEG/EMG

All surgical procedures implemented in this study were as previously published (27). Briefly, subdural EEG and suprascapular EMG electrode implantation was performed under isoflurane anesthesia (4%–1.5%). We used coordinates from bregma for consistent placement of the EEG screw electrodes (Supplemental Figure S1), as previously published (18). After recovering from electrode implantation surgery (mean \pm SD = 7 \pm 1 day), mice were placed in a recording chamber with food and water provided ad libitum. Wild-type (WT^{+/+}) and *Syngap1*^{+/-} mice underwent 24-hour video EEG/EMG recording at younger (P60, WT^{+/+} n = 4, Het^{+/-} n = 6) and older (P90–P120; WT^{+/+} n = 4, Het^{+/-} n = 7) ages. For further details of EEG acquisition parameters, see Supplement.

Hypnogram and EEG Power Analysis

EEG data were manually scored for wake, non-rapid eye movement (NREM), and rapid eye movement (REM) states for every 10-second epoch by a scorer blinded to genotype and sex. All artifacts identified on EEG underwent video confirmation and were removed from all further analyses. All EEG power analysis protocols used in this study were as previously published (27,28). For further details, see Supplement.

Seizure and IIS Scoring

Spontaneous seizures were identified by manual review of all 24-hour EEGs by a scorer blinded to genotype and sex. IISs were visually analyzed on raw EEGs using conservative parameters obtained from obvious pre- and post-ictal spikes for every 5-second EEG epoch. For further details on seizure and IIS scoring parameters, see Supplement.

Analysis of Human EEG Recording

Continuous overnight EEGs were acquired with parental consent under an approved institutional review board protocol (29). The EEG channels F4, C4, and O2 were re-referenced to A1 or A2 and exported in the European Data File format, de-identified, and assigned an identification number. Each epoch was manually scored as wake, NREM, or REM, as previously published (17). Seizure scoring was performed separately from sleep scoring. For further details, see Supplement.

Immunohistochemistry

One week after the final EEG recordings (P127), mice were anesthetized with chloral hydrate (300 mg/mL intraperitoneally), followed by transcardiac perfusion with ice-cold phosphate-buffered saline solution and subsequent fixation with 10% formalin. Brains were subsequently cryoprotected and stored at -80°C before cryosectioning. All coronal sections were cut at 14 μm and mounted onto Superfrost Plus microscope slides (Thermo Fisher Scientific, Waltham, MA) before staining. Fluorescent images were acquired at $\times 10$ and $\times 40$ using Z-stacks with Axiovision Software 4.6 and Apotome (Carl Zeiss, Jena, Germany). All data analyses were performed using ImageJ software (30). All data were analyzed by a scorer blinded to genotype and sex. For further details, see Supplement.

Statistical Analyses

Statistical tests were performed using Prism 8.3 (GraphPad Software, La Jolla, CA). All 1-way and 2-way analyses of variance (ANOVAs) were performed with Bonferroni post hoc corrections. All independent *t* tests and nested *t* tests were 2 tailed. All data are reported as mean \pm 1 SEM. For further details, see Supplement.

RESULTS

Syngap1^{+/-} Mice Have Recurrent Spontaneous Seizures With Multiple Phenotypes

Continuous 24-hour video EEG/EMG recordings at temporally advancing ages identified spontaneous seizures in 50% of *Syngap1*^{+/-} mice (n = 4 of 8 mice) (Figure 1). At P60 all

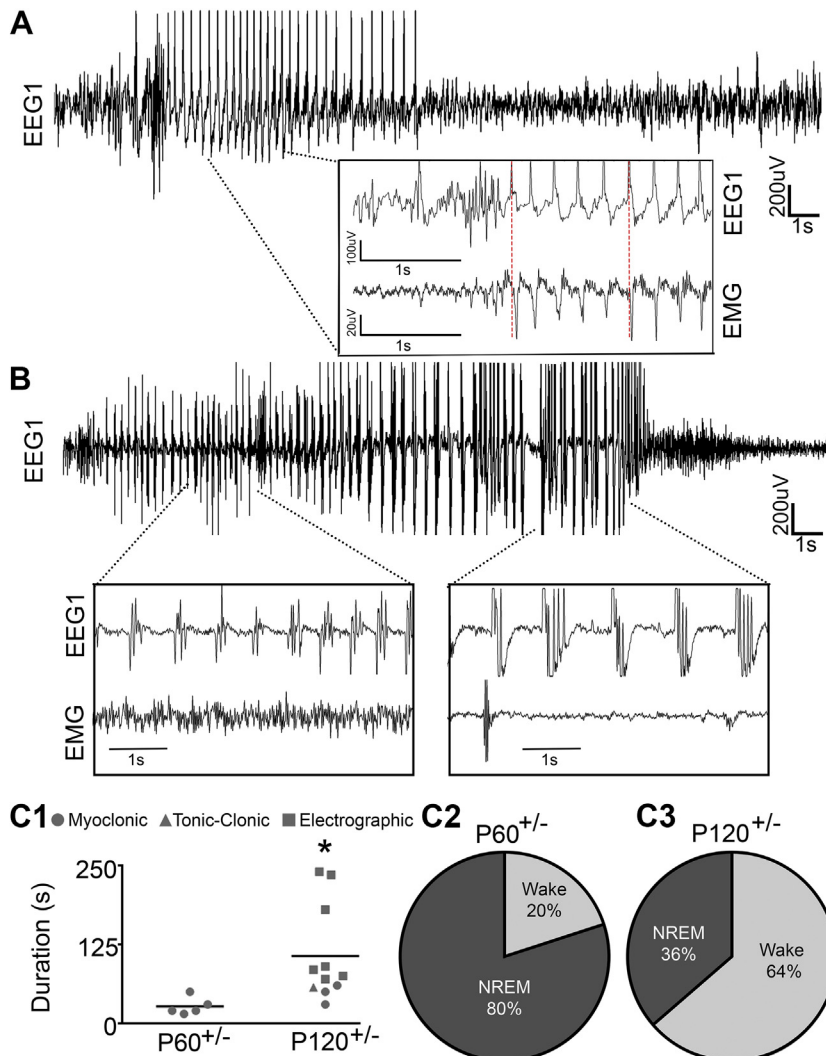


Figure 1. *Syngap1*^{+/-} mice had recurrent spontaneous seizures. **(A)** Representative EEG trace (0.5–50 Hz) of a spontaneous myoclonic seizure at P60 during NREM sleep (P60 EEG recordings, $n = 6$ *Syngap1*^{+/-} mice). Prototypical time-locked myoclonic jerks were recorded on EMG (Supplemental Video). **(B)** Representative spontaneous tonic-clonic seizure at P120 during NREM sleep (P120 EEG recordings, $n = 7$ *Syngap1*^{+/-} mice). **(C1)** Multiple seizure phenotypes emerged at P120, and the average duration of seizures significantly increased from P60 to P120 (t test, $t_{14} = 2.307$, $p = .037$). **(C2)** At P60, all seizures were myoclonic and the majority (4/5 seizures, $n = 2$ mice) occurred during NREM. **(C3)** At P120, all myoclonic (3/11 seizures, $n = 3$ mice) and tonic-clonic (1/11 seizures, $n = 1$ mouse) seizures occurred during NREM, whereas all electrographic seizures occurred during wake (7/11 seizures, $n = 3$ mice) (for the electrographic seizure trace, see Supplemental Figure S2). * $p < .05$, post hoc Bonferroni correction. EEG, electroencephalography; EMG, electromyography; NREM, non-rapid eye movement; P, postnatal day.

seizures were myoclonic ($n = 5$ of 5 seizures); 80% of these seizures ($n = 4$ of 5) started in NREM at transitions from NREM to wake (Figure 1A). Myoclonic seizures were 34.4 ± 5.9 seconds in duration with ~ 3 –4-Hz rhythmic spike-wave discharges (Figure 1A), which was similar to clinical reports (12). The myoclonic seizures were distinguished by their time-locked myoclonic jerks recorded on EMG with video confirmation of head, neck, and upper shoulder myoclonic jerks (Supplemental Video).

Multiple seizure phenotypes were identified in *Syngap1*^{+/-} mice at P120, which was consistent with the latest clinical reports (12,31). Myoclonic, generalized tonic-clonic, and electrographic seizures were observed (Figure 1B, C; Supplemental Figure S2). All myoclonic seizures ($n = 3$ of 11 seizures) and tonic-clonic seizures ($n = 1$ of 11 seizures) occurred during NREM in *Syngap1*^{+/-} mice at P120, whereas all electrographic seizures occurred during wake ($n = 7$ of 11 seizures) (Figure 1C3). Electrographic (subclinical) seizures were distinguished by their abnormal EEG patterns that were apparent

only on EEG and not associated with any behavioral change. Myoclonic seizures had a propensity to emerge during NREM regardless of age. From P60 to P120, the average seizure duration significantly increased from 27 ± 0.6 seconds to 106 ± 22.7 seconds (Figure 1C1). This increase in seizure duration was driven by the emergence of electrographic seizures at P120.

Recurrent Generalized Seizures in Human SYNGAP1 Haploinsufficiency Show Affinity for Transition States and Clustering in NREM

To evaluate the translational value of 24-hour qEEG analysis in *Syngap1*^{+/-} mice, 2 EEG recordings from children diagnosed with SYNGAP1 haploinsufficiency-related epilepsy were acquired (29) and analyzed. A 20-hour continuous EEG captured an entire cycle of overnight sleep in a 3-year-old boy with SYNGAP1 haploinsufficiency (Figure 2). Global seizures were identified as bursts of 3–4-Hz spikes and slow waves that lasted ~ 0.5 –3 seconds (Figure 2A). All ictal events observed

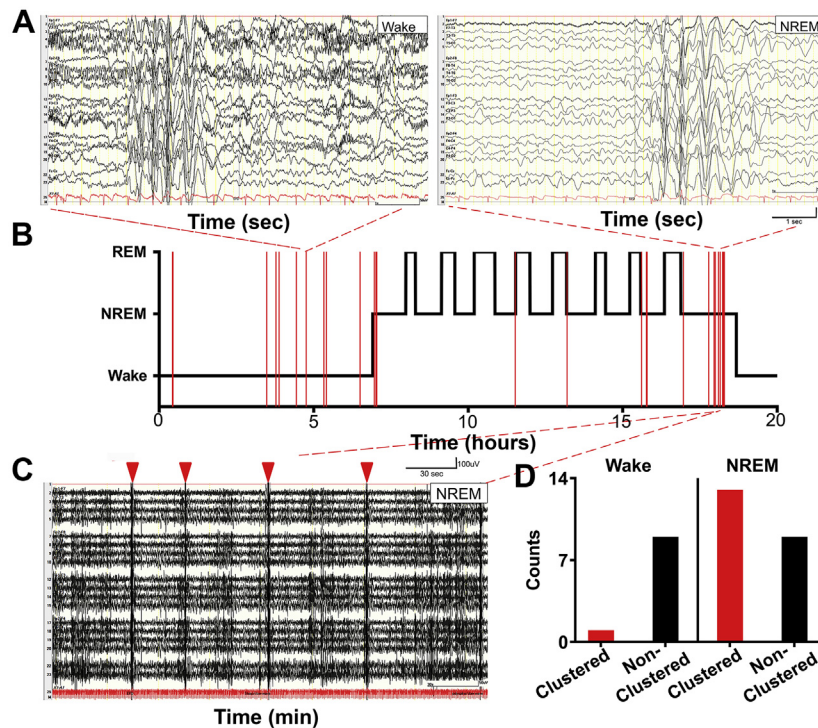


Figure 2. Ictal events during a 20-hour overnight EEG recording in a 3-year-old boy with *SYNGAP1* haploinsufficiency. **(A)** Identical 3-Hz short-duration epileptiform events during wake and NREM sleep. **(B)** Hypnogram for the 20-hour period, with clustering of events identified during NREM sleep. **(C)** 5-minute EEG trace showed four clustered events (red arrowheads) occurring within a 5-minute period during the last NREM cycle before wake. Note ictal events occurring at transition points between wake-NREM and REM-NREM (for a 50-minute EEG recorded from a 5-year-old girl with *SYNGAP1* haploinsufficiency, see *Supplemental Figure S3*). **(D)** Bar graphs grouping clustered vs. nonclustered events for wake and NREM showed affinity for ictal clustering during NREM ($n = 1$, a 3-year-old-boy with *SYNGAP1* haploinsufficiency). Seizure rates normalized per hour of EEG recording in the raster were wake = 1.27/hour, NREM = 2.68/hour, and REM = 0/hour. EEG, electroencephalography; NREM, non-rapid eye movement; REM, rapid eye movement.

during sleep occurred in NREM (Figure 2B), and an affinity for clustering of ictal events (i.e., interictal durations <5 minutes) during NREM was noted (Figure 2C, D). Furthermore, ictal events predominantly occurred during wake-NREM and NREM-REM transitions. A 50-minute clinical EEG recorded from a 5-year-old girl diagnosed with *SYNGAP1* haploinsufficiency showed a similar clustering of generalized ~3–4-Hz short-duration seizures during transitions from wake to first NREM (Supplemental Figure S3). These observations identified a previously undescribed clustering of ictal events during NREM and the propensity of the ictal clusters to occur during transitions between behavioral states.

Progressive Alterations in Sleep Macro-architecture

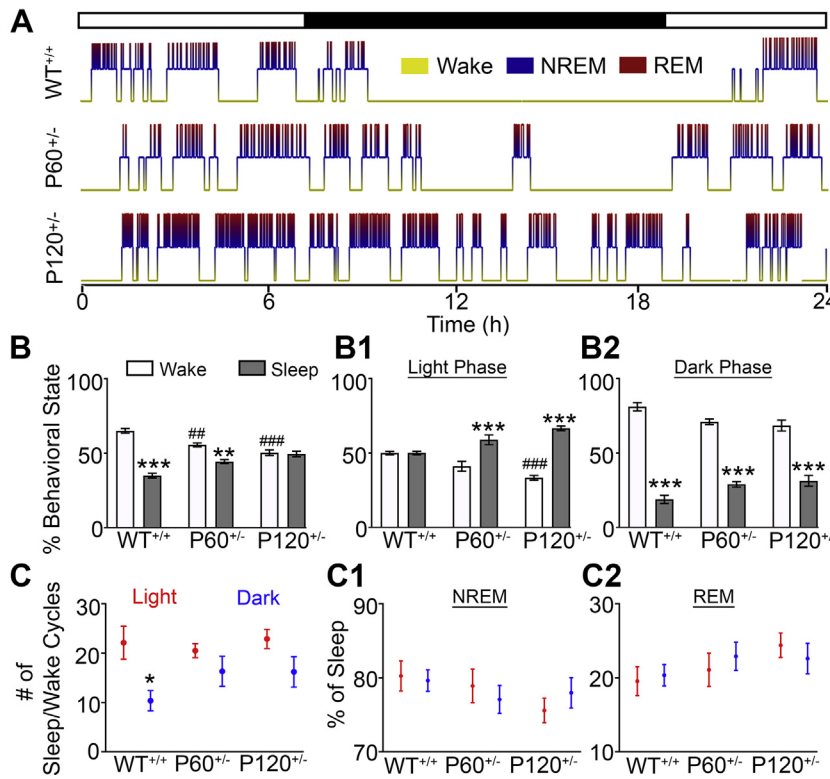
Sleep dysfunction is a common feature of NDDs and is reported in patients with *SYNGAP1* haploinsufficiency (12,21). Quantitative assessments of the sleep problems in patients with *SYNGAP1* haploinsufficiency are lacking, so future assessments will be informative (29). In the present study, the *WT^{+/+}* sleep macro-architecture was ultradian with 15.38 ± 2.2 sleep cycles occurring over 24 hours (Figure 3A). All *WT^{+/+}* mice, regardless of age, demonstrated a consistent sleep architecture (Supplemental Figure S4). *WT^{+/+}* mice spent ~80% of the time awake during the dark phase (Figure 3A, B2), demonstrating the nocturnal predominance of activity in *WT^{+/+}* mice. Between groups, *P60^{+/−}* and *P120^{+/−}* mice spent more time asleep than *WT^{+/+}* mice over 24 hours (Figure 3B). Compared with *WT^{+/+}* mice, *P120^{+/−}* mice spent significantly more time asleep during the light phase (Figure 3B1). In *WT^{+/+}*

mice, there were significantly fewer sleep/wake cycles during the dark phase (10.37 ± 2.0 cycles) compared with the light phase (22.13 ± 3.3 cycles) (Figure 3C). In *P60^{+/−}* and *P120^{+/−}* mice, the difference between the numbers of sleep/wake cycles during light versus dark phase was not significant (Figure 3C). In contrast to the significant differences in sleep macro-architecture, all mice maintained a sleep micro-architecture of ~80% NREM and ~20% REM during the 24-hour recordings (Figure 3C1, C2).

IISs Predominantly Occurred During NREM Sleep and Were Progressive With Age

Uncontrolled epilepsy is at least partially responsible for cognitive regression in children with epileptic encephalopathies (19,20). All *Syngap1^{+/−}* mice presented IISs during both sleep and wake (Figure 4A, B). IIS frequency significantly increased in *P120^{+/−}* mice compared with *WT^{+/+}* mice (1-way ANOVA, $F_{2,20} = 4.278$, $p = .0284$). This significant increase was driven by IISs that occurred during NREM sleep, specifically during light-phase sleep (Figure 4C, D). Furthermore, even though the total duration of sleep increased significantly in *P120^{+/−}* mice (Figure 3B), the rate of IIS occurrence per hour of NREM sleep was significantly greater in *P120^{+/−}* compared with *WT^{+/+}* mice (Figure 4D).

Emerging research using intracranial recordings from epilepsy patients has demonstrated that regulation of brain activity occurs on long time scales (32). Daily patterns of seizure occurrence demonstrate circadian rhythmicity and clustering organization (32). In the present study, we report the relationship between seizure occurrence and frequency distribution of



cantly fewer cycles (transitions between sleep and wake) during the dark phase than during the light phase ($WT^{+/+}$ light cycles vs. $WT^{+/+}$ dark cycles: 2-way ANOVA, $F_{2,40} = 0.998$, $p = .04$). (C1, C2) Although the significant diurnal difference in the number of sleep/wake cycles detected in $WT^{+/+}$ did not occur in $P60^{+/-}$ and $P120^{+/-}$ mice, the micro-architecture of both NREM and REM cycles during sleep was not significantly different. $WT^{+/+}$ $n = 6$, $P60^{+/-}$ $n = 6$, $P120^{+/-}$ $n = 7$. * $p < .05$, ** $p < .01$, *** $p < .001$, # $p < .05$, ## $p < .01$, ### $p < .001$, post hoc Bonferroni corrections. ANOVA, analysis of variance; NREM, non-rapid eye movement; P, postnatal day; P60^{+/-}, *Syngap1*^{+/-} mice at postnatal day 60; P120^{+/-}, *Syngap1*^{+/-} mice at postnatal day 120; REM, rapid eye movement; WT, wild-type.

IISs over 24 hours for all mice (Figure 4E, F). Grouped data of IIS frequency averaged over 24 hours showed an escalation in IIS frequency at the beginning of the light phase and was associated with an increased incidence of seizures in $P120^{+/-}$ mice. Antagonizing AMPARs acutely with PMP (2 mg/kg intraperitoneally at 10 AM and 6 PM) prevented seizures during the 24-hour EEG but did not significantly reduce IIS frequency (Supplemental Figure S5). In summary, IIS occurrence was greatest during NREM in *Syngap1*^{+/-} mice.

Hyperactivity Worsened With Age

Video tracking software allows for high specificity and sensitivity when tracking mouse motor activity over the 24-hour recordings. Total distance traveled by each mouse over a 24-hour period was used to identify hyperactivity in *Syngap1*^{+/-} mice (Figure 5A). Compared with $WT^{+/+}$ mice (267.92 ± 46.8 m), $P120^{+/-}$ mice traveled greater distances (479.75 ± 46.1 m), which was not detected in the $P60^{+/-}$ mice (288.22 ± 32 m) (Figure 5A2, A3). Since $P120^{+/-}$ mice spent more time asleep than $WT^{+/+}$ mice (Figure 3), the distance traveled by each mouse was normalized to the duration of time spent asleep. The running average of mice in each group highlighted increased activity at the end of the dark phase, when the majority of nesting behavior occurs (33) (Figure 5B). The

Figure 3. Progressive alterations in sleep macro-architecture. (A) 24-hour hypnograms of nocturnal ultra-radian rhythms in $WT^{+/+}$, $P60^{+/-}$, and $P120^{+/-}$ mice. Regardless of age, all $WT^{+/+}$ mice had consistent sleep macro- and micro-architectures (Supplemental Figure S4). (B) $WT^{+/+}$ mice spent significantly less time asleep than awake ($WT^{+/+}$ wake vs. $WT^{+/+}$ sleep: 2-way ANOVA, $F_{2,40} = 42.01$, $p < .0001$). $P60^{+/-}$ mice also spent significantly less time asleep than awake ($P60^{+/-}$ wake vs. $P60^{+/-}$ sleep: 2-way ANOVA, $F_{2,40} = 42.01$, $p = .002$). In contrast, $P120^{+/-}$ mice lacked any significant differences between durations of wake and sleep. Between groups, time spent awake significantly decreased in $P60^{+/-}$ mice ($WT^{+/+}$ wake vs. $P60^{+/-}$ wake: 2-way ANOVA, $F_{2,40} = 42.01$, $p = .009$) and $P120^{+/-}$ mice ($WT^{+/+}$ wake vs. $P120^{+/-}$ wake: 2-way ANOVA, $F_{2,40} = 42.01$, $p < .0001$). (B1) During the 12-hour light phase, in contrast to $WT^{+/+}$, both $P60^{+/-}$ and $P120^{+/-}$ mice spent more time asleep than awake ($P60^{+/-}$ light wake vs. $P60^{+/-}$ light sleep: 2-way ANOVA, $F_{2,40} = 40.07$, $p < .0001$; $P120^{+/-}$ light wake vs. $P120^{+/-}$ light sleep, $p < .0001$). The amount of time $P120^{+/-}$ mice spent awake was significantly lower than that of $WT^{+/+}$ mice ($WT^{+/+}$ light wake vs. $P120^{+/-}$ light wake: $F_{2,40} = 40.0$, $p < .0001$). (B2) $WT^{+/+}$, $P60^{+/-}$, and $P120^{+/-}$ mice all spent significantly less time asleep than awake during the dark phase ($WT^{+/+}$ dark sleep vs. $WT^{+/+}$ dark wake: 2-way ANOVA, $F_{2,40} = 9.617$, $p < .0001$; $P60^{+/-}$ dark wake vs. $P60^{+/-}$ dark sleep: $p < .0001$; $P120^{+/-}$ dark wake vs. $P120^{+/-}$ dark sleep: $p < .0001$). (C) Only $WT^{+/+}$ mice had significantly fewer cycles (transitions between sleep and wake) during the dark phase than during the light phase ($WT^{+/+}$ light cycles vs. $WT^{+/+}$ dark cycles: 2-way ANOVA, $F_{2,40} = 0.998$, $p = .04$). (C1, C2) Although the significant diurnal difference in the number of sleep/wake cycles detected in $WT^{+/+}$ did not occur in $P60^{+/-}$ and $P120^{+/-}$ mice, the micro-architecture of both NREM and REM cycles during sleep was not significantly different. $WT^{+/+}$ $n = 6$, $P60^{+/-}$ $n = 6$, $P120^{+/-}$ $n = 7$. * $p < .05$, ** $p < .01$, *** $p < .001$, # $p < .05$, ## $p < .01$, ### $p < .001$, post hoc Bonferroni corrections. ANOVA, analysis of variance; NREM, non-rapid eye movement; P, postnatal day; P60^{+/-}, *Syngap1*^{+/-} mice at postnatal day 60; P120^{+/-}, *Syngap1*^{+/-} mice at postnatal day 120; REM, rapid eye movement; WT, wild-type.

normalized distance traveled by $P120^{+/-}$ mice was significantly greater than that of the $WT^{+/+}$ and $P60^{+/-}$ mice (Figure 5C). $P120^{+/-}$ mice spent more time asleep but were hyperactive when awake, as they traveled twice the distance of $WT^{+/+}$ mice. These results are consistent with recent reports of home-cage hyperactivity in male *Syngap1*^{+/-} mice (34,35).

Activity-Dependent Theta Modulation Is Impaired During Wake in $P120^{+/-}$ Mice

Cross-frequency coupling occurs between theta and gamma oscillations (36,37). Specifically, gamma oscillations are nested within theta oscillations (38,39) and are critical for memory retrieval (40–42). To determine differences in theta and gamma power during transitions from stationary to active wake, 10-minute epochs were analyzed (Figure 6A). During stationary wake, high theta and low gamma power were apparent in $WT^{+/+}$ mice (Figure 6A–B). After the transition to active wake, $WT^{+/+}$ mice had high gamma and low theta power. The state-dependent (stationary vs. active wake) modulation of theta power was not apparent in $P120^{+/-}$ mice (Figure 6B, C).

In $WT^{+/+}$ mice, theta and gamma spectral power demonstrated an inverse relationship during wake-sleep state transitions (Supplemental Figure S6A). During wake, the theta:gamma ratio was low in $WT^{+/+}$ mice, while during sleep the theta:gamma ratio

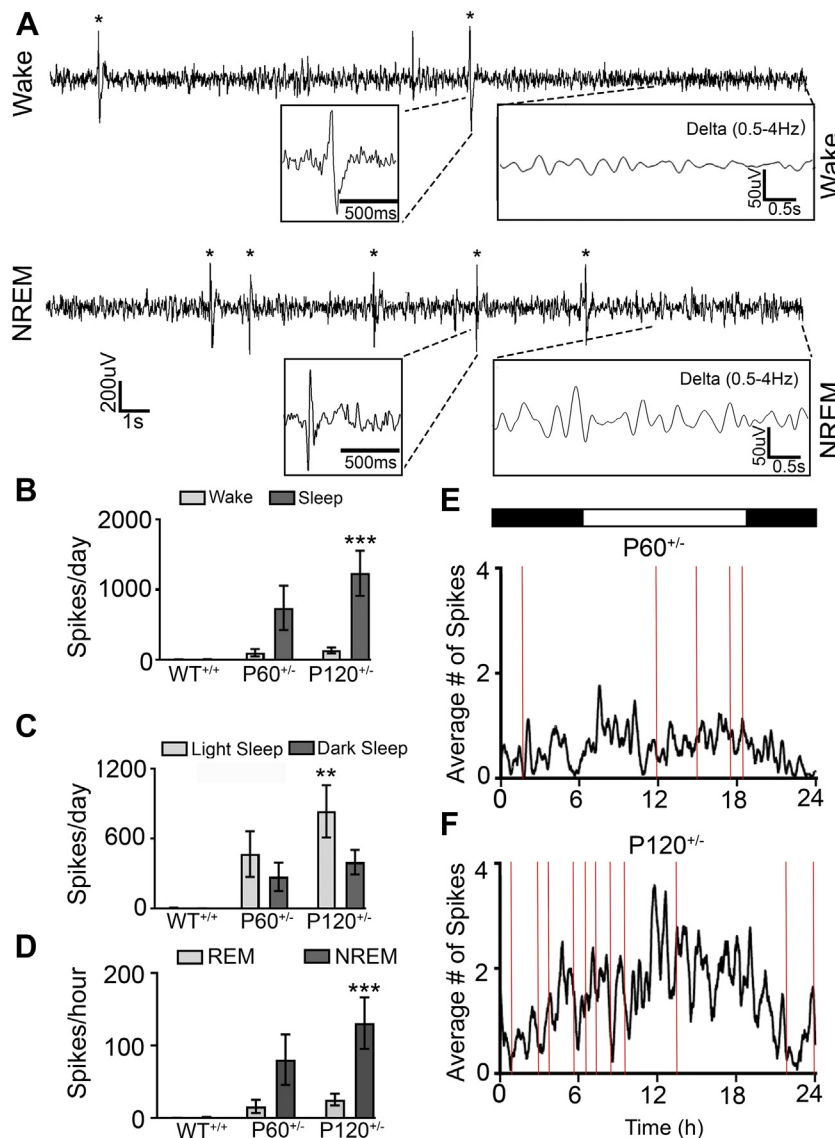


Figure 4. Progressive interictal spiking during NREM. **(A)** 30-second EEG trace (0.5–50 Hz) during wake of interictal spikes ($n = 2$ spikes; black asterisks) with low amplitude delta power (0.5–4 Hz). During NREM sleep, a 30-second EEG trace demonstrated interictal spikes ($n = 5$ spikes, asterisks) with high-amplitude delta power (0.5–4 Hz). **(B)** Number of spikes during sleep significantly increased in P120^{+/-} compared with WT^{+/+} mice (WT^{+/+} sleep spikes vs. P120^{+/-} sleep spikes: 2-way analysis of variance, $F_{2,40} = 4.80$, $p = .0003$). **(C)** Number of spikes significantly increased during light sleep in P120^{+/-} mice (WT^{+/+} light sleep spikes vs. P120^{+/-} light sleep spikes: 2-way analysis of variance, $F_{2,40} = 1.33$, $p = .0012$). **(D)** Interictal spikes significantly increased with age during NREM (WT^{+/+} NREM spikes vs. P120^{+/-} NREM spikes: 2-way analysis of variance, $F_{2,40} = 3.508$, $p = .0006$). **(E, F)** Interictal spikes (black traces) and seizure frequency (red lines) over 24 hours. WT^{+/+} $n = 6$ mice, P60^{+/-} $n = 6$ mice, P120^{+/-} $n = 7$ mice. * $p < .05$, ** $p < .01$, **** $p < .001$, post hoc Bonferroni corrections. EEG, electroencephalography; NREM, non-rapid eye movement; P, postnatal day; PMP^{+/+}, PMP administered Syngap1^{+/-} mice; P120^{+/-}, Syngap1^{+/-} mice at postnatal day 120; WT, wild-type.

was high (Supplemental Figure S6A) (43,44). This relationship between theta and gamma power was lost in *Syngap1^{+/-}* mice at P120 (Supplemental Figure S6).

Loss of Behavioral-State Homeostasis of Cortical Gamma

High cognitive load during wakefulness (45–47) is associated with increased gamma power. Accordingly, in WT^{+/+} mice gamma power was high during wake and low during NREM sleep (Figure 7A). P120^{+/-} mice did not demonstrate this behavioral state-dependent gamma power modulation during wake-NREM transitions, as gamma power remained high during NREM (Figure 7B). PMP-treated *Syngap1^{+/-}* mice showed a significant rescue of the gamma dysregulation: high gamma during wake and low gamma during NREM similar to

WT^{+/+} mice (Figure 7C). In WT^{+/+} mice the slopes of gamma power during wake-NREM transitions over 24 hours were negative, as gamma power decreased during NREM. During NREM-wake transitions, the slope of gamma power was positive in WT^{+/+} mice as gamma power increased during wake (Figure 7D1). These negative slopes of wake-NREM transitions and positive slopes of NREM-wake transitions were significantly different from one another in WT^{+/+} mice (Figure 7D1), whereas P120^{+/-} mice failed to show significant differences between gamma slopes (Figure 7D2). PMP significantly rescued the transition state-dependent differences between the slopes of gamma power in the Het^{+/-} mice (Figure 7D3). The average gamma slopes for both wake-NREM and NREM-wake transitions were compared between groups (Supplemental Figure S7). Mean gamma slopes between NREM-wake and wake-NREM transitions

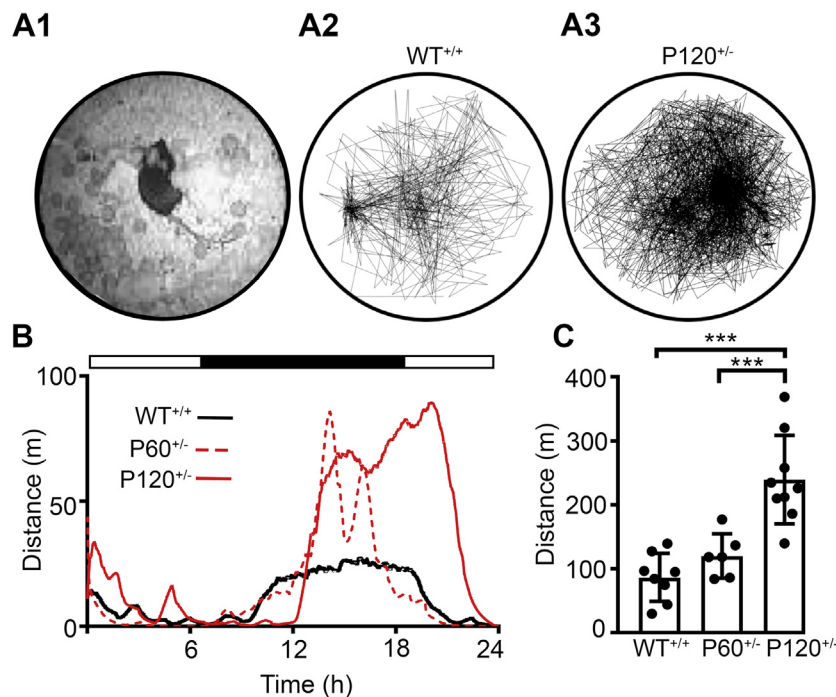


Figure 5. Progressive increase in activity during 24-hour recordings. **(A1)** Image from the infrared top-view camera used for motion tracking. **(A2, A3)** Representative traces of WT^{+/+} and P120^{+/−} activity over 24 hours within individual recording chambers. **(B)** A representative local regression for distance traveled over 24 hours by a WT^{+/+}, a P60^{+/−}, and a P120^{+/−} mouse. All of the mice showed increased activity during the exploration and nesting phase. **(C)** P120^{+/−} mice showed significantly higher activity than WT^{+/+} and P60^{+/−} mice (WT^{+/+} vs. P120^{+/−}: 1-way analysis of variance; $F_{2,20} = 20.18$, $p < .001$; P120^{+/−} vs. P60^{+/−}: $p < .001$). WT^{+/+} $n = 6$, P60^{+/−} $n = 6$, P120^{+/−} $n = 7$. * $p < .05$, ** $p < .01$, *** $p < .001$, post hoc Bonferroni corrections. P, postnatal day; P60^{+/−}, *Syngap1*^{+/−} mice at postnatal day 60; P120^{+/−}, *Syngap1*^{+/−} mice at postnatal day 120; WT, wild-type.

in WT^{+/+} mice were significantly different, and were lost in P120^{+/−} mice. PMP rescued this loss in the *Syngap1*^{+/−} mice (*Supplemental Figure S7*). Furthermore, low-dose PMP did not significantly alter cortical gamma during transitions between wake and sleep in the WT^{+/+} mice that were administered PMP (*Supplemental Figure S8*).

Additional analyses of binned gamma power were undertaken because spectral frequency analysis identified that the significant behavioral-state alterations in gamma power modulation between NREM and wake in P120^{+/−} mice were predominantly driven within the 35–45-Hz range (*Supplemental Figure S9*). Power in the 35–45-Hz bin was significantly higher during wake compared with NREM in WT^{+/+} mice (*Supplemental Figure S9*), which was lost and reversed in P120^{+/−} mice (*Supplemental Figure S9*). In summary, *Syngap1*^{+/−} mice showed a loss of state-dependent gamma modulation.

During NREM, the majority of brain activity is synchronous slow-wave activity with low gamma power (45–47). In contrast, gamma power increases during the asynchronous activity of REM (45–47), hence its description as paradoxical sleep. In WT^{+/+} mice, NREM-REM transitions underwent modulation in gamma, theta, and delta powers (*Figure 8*). A significantly lower percentage of change in gamma power during NREM-REM transitions was apparent in P120^{+/−} mice when compared with WT^{+/+} mice. This impairment in gamma power modulation from NREM to REM was significantly rescued by PMP (*Figure 8B*).

Deficits in Parvalbumin-Positive Interneuron Innervation in the Prefrontal Cortex

The majority of perisomatic inhibition is mediated by parvalbumin-positive interneurons (PV⁺ INs) (45), which have a

significant role in the modulation of cortical gamma oscillations (48). Our novel finding of consistently high gamma power in *Syngap1*^{+/−} mice directed the investigation of the density distribution of PV⁺ INs in the cerebral cortex, hippocampus, and prefrontal cortices. PV⁺ IN distributions did not show significant differences in overall densities in either the dorsal pallidum cortex (DP) (WT^{+/+} vs. Het^{+/−}: nested *t* test, $t_{14} = 0.6823$, $p = .51$) or the prelimbic cortex (PrL) (WT^{+/+} vs. Het^{+/−}: nested *t* test, $t_{14} = 0.5755$, $p = .46$). The quantification of total and perisomatic PV⁺ puncta counts identified significant deficits in the DP cortex of *Syngap1*^{+/−} mice (*Figure 9A, B*), but not in the PrL cortex (PrL total PV counts, WT^{+/+} vs. Het^{+/−}: nested *t* test, $t_{14} = 0.055$, $p = .95$; PrL soma PV counts, WT^{+/+} vs. Het^{+/−}: $t_{14} = 1.434$, $p = .1734$). GluA2 fluorescence intensity on PV⁺ IN somas (putative Ca²⁺-impermeable AMPARs) and non-PV⁺ neurons showed no significant differences in DP (*Figure 9C, D*) (for antibody verification see *Supplemental Figure S10*) or PrL. These findings indicate that deficits in PV⁺ IN innervation were region specific within the prefrontal cortex in *Syngap1*^{+/−} mice.

These findings warranted the analysis of PV⁺ puncta counts in other regions of interest. Unlike the prefrontal cortex, no significant differences in PV⁺ puncta count were noted in either the barrel cortex (BCX) or motor cortex (*Figure 10A1, B1*). A layer-specific investigation of BCX and motor cortex demonstrated that PV⁺ puncta counts were not significantly different between layers for both the total counts and the non-PV⁺ somas (*Figure 10A1, B1*). In the hippocampus, PV⁺ puncta counts were not significantly different in the CA1 or CA3 regions (*Figure 10C1*). Normalized PV⁺ puncta counts in the CA1 and CA3 regions were not significantly different between the stratum pyramidale, stratum radiatum, or stratum

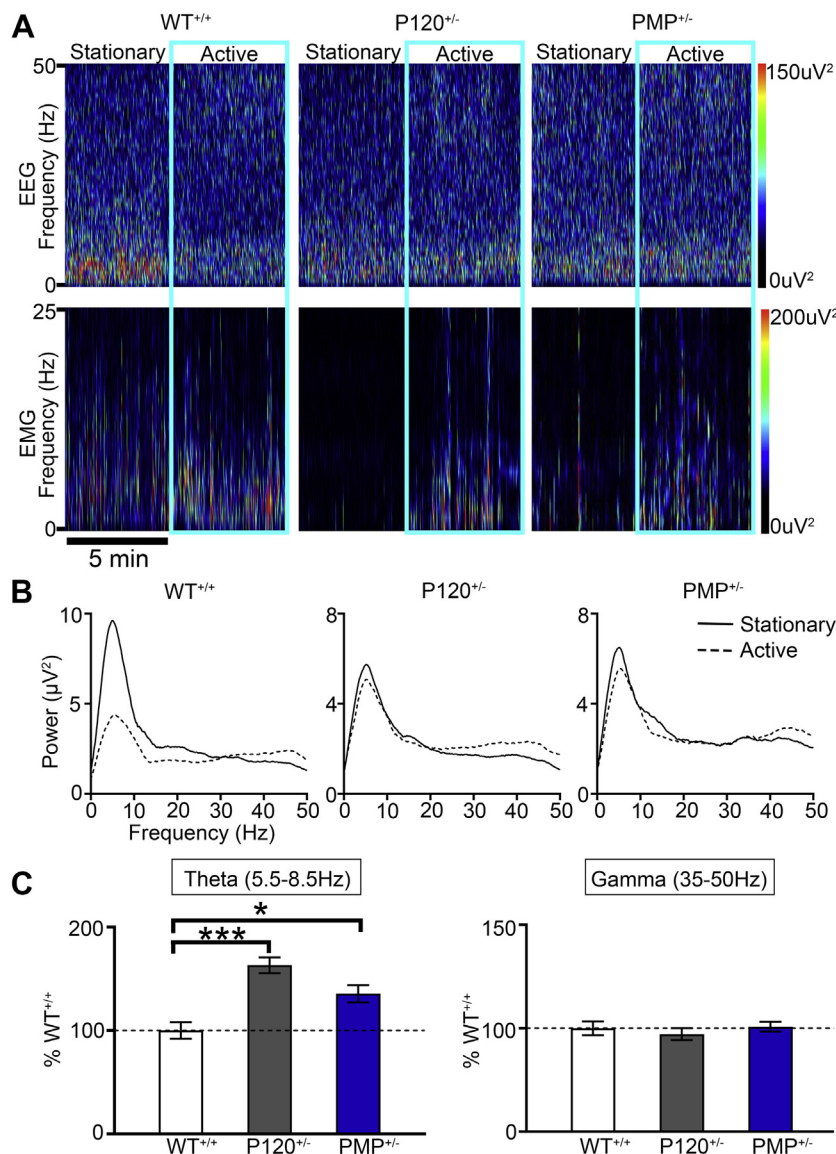


Figure 6. Progressive impairment of theta power during transitions from inactive to active wake. **(A)** EEG and EMG spectral power heat maps of activity-dependent transitions from stationary to active wake in WT^{+/+} mice. P120^{+/-} mice failed to demonstrate an increase in gamma with concurrent decrease in theta. **(B)** Representative spectral frequency traces in WT^{+/+} and P120^{+/-} mice during transitions from inactive to active wake. **(C)** The lack of theta modulation in P120^{+/-} mice during transitions from inactive to active wake was significant (WT^{+/+} theta % vs. P120^{+/-} theta %: 1-way analysis of variance, $F_{2,22} = 13.51, p < .0001$). PMP administration (2 mg/kg intraperitoneally) at 10 AM and 6 PM failed to significantly rescue theta modulation with acute dosing (WT^{+/+} theta % vs. PMP^{+/-} theta %: 1-way analysis of variance, $F_{2,22} = 13.51, p = .017$). During transitions from inactive to active wake, gamma modulation was not significantly impaired. WT^{+/+} $n = 6$, P60^{+/-} $n = 6$, P120^{+/-} $n = 7$, PMP^{+/-} $n = 4$. * $p < .05$, ** $p < .01$, *** $p < .001$, post hoc Bonferroni corrections. EEG, electroencephalography; EMG, electromyography; P, postnatal day; P120^{+/-}, *Syngap1*^{+/-} mice at postnatal day 120; PMP, perampanel; PMP^{+/-}, PMP administered *Syngap1*^{+/-} mice; WT, wild-type.

oriens of WT^{+/+} and Het^{+/-} mice at P120. In summary, deficits in PV⁺ innervation were observed only in the DP cortex.

Increased GluA2 Expression on PV⁺ Soma in Somatosensory but Not Motor Cortex

A rich diversity of GABAergic (gamma-aminobutyric acidergic) neurons shape the spatiotemporal dynamics of cortical circuit outputs by elegant inhibitory control mechanisms (49,50). As reported by previous research, compared with pyramidal neurons, PV⁺ INs have a lower expression profile for the GluA2 subunit (51). PV⁺ INs in both L2–3 and L5–6 of the BCX showed significant upregulation of GluA2 (Figure 10A2), which was absent in the motor cortex (Figure 10B2). The mean GluA2 fluorescence intensity on PV⁺ INs was also significantly higher in the CA3 region but not in the CA1 region (Figure 10C2). No

significant differences in GluA2 fluorescence intensities were noted in the non-PV⁺ cells in any region of interest that was investigated (Supplemental Figure S11). Since all *Syngap1*^{+/-} mice were epileptic, the hippocampi were investigated for mossy fiber sprouting. No evidence for mossy fiber sprouting was detected in this model (Supplemental Figure S12). In summary, a significant region-specific upregulation of GluA2 expression in PV⁺ INs, a population of INs known to generate cortical gamma oscillations (48), was detected in *Syngap1*^{+/-} mice.

DISCUSSION

Continuous EEG monitoring for 24 hours and qEEG protocols (27) identified novel biomarkers underlying epileptogenesis in a mouse model of *Syngap1* haploinsufficiency. Progressive

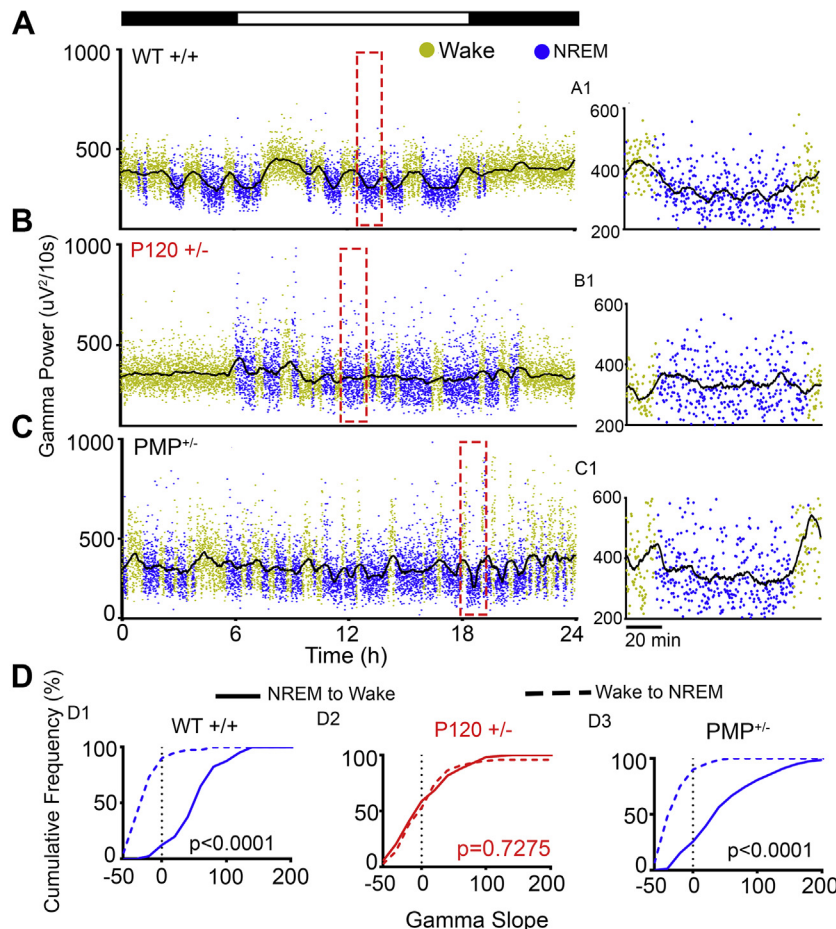


Figure 7. Gamma during transitions between wake and NREM behavioral state modulation of EEG gamma spectral power. **(A)** 24-hour WT^{+/-} gamma traces had high gamma during wake and low gamma during NREM. **(A1)** Expanded time scale [red boxes in **(A–C)** expanded in **(A1–C1)**] shows a gradual fall of gamma from wake to NREM and gradual rise of gamma from NREM to wake. **(B)** Gamma power in the P120^{+/-} mice failed to transition to NREM levels; **(B1)** expanded time scale demonstrates the failure of gamma attenuation during an NREM cycle. **(C, C1)** In PMP^{+/-}, behavioral-state transitions in gamma power were significantly rescued. **(D)** Cumulative frequency graphs of positive NREM-to-wake slopes and negative wake-to-NREM slopes in WT^{+/-}. **(D1)** These slopes were significantly different (t test, $t_{275} = 10.59$, $p < .001$) between the two independent transition states. **(D2)** No behavioral state-dependent modulation of gamma power occurred in P120^{+/-} mice (t test, $t_{327} = 0.3488$, $p = .7275$). **(D3)** PMP administration restored behavioral-state-dependent gamma power modulation (t test, $t_{156} = 9.854$, $p < .0001$). WT^{+/-} $n = 6$, P120^{+/-} $n = 7$, PMP^{+/-} $n = 4$. NREM, non-rapid eye movement; P, postnatal day; P120^{+/-}, *Syngap1*^{+/-} mice at postnatal day 120; PMP, perampanel; PMP^{+/-}, PMP administered *Syngap1*^{+/-} mice; WT, wild-type.

worsening in epileptogenesis, IIS frequency, hyperactivity, and impaired behavioral-state dependent modulation of cortical gamma activity during both wake- and sleep-state transitions were identified. Myoclonic ~3-Hz seizures in the *Syngap1*^{+/-} mice arose during NREM sleep. Human overnight and clinical EEG analyses identified ictal clusters of 3-Hz spike-wave discharges during NREM that were aggravated at transitions from wake to sleep and sleep to wake. Currently, it is unknown if any other models of *Syngap1* haploinsufficiency that differ by mutation site or mutation strategy (i.e., germ-line vs. Cre recombinase) show these clinically relevant 3-Hz seizures with progression to multiple other phenotypes. In addition, the rescue of impaired cortical gamma homeostasis during behavioral-state transitions by PMP identified the critical role of AMPARs in such transitions. Induced increase of GluA2 expression in INs resulted in severe disruption of gamma oscillations (52). This previous research implicated the Ca²⁺-impermeable AMPAR subunit, which confers a slow excitatory postsynaptic potential in excitatory neurons and is usually expressed at low levels in GABAergic INs (52), in playing a critical role in gamma power during behavioral-state transitions. Immunolabeling identified excessive GluA2-AMPAR

expression on the somas of PV⁺ INs in *Syngap1*^{+/-} mice that was location specific, supporting our hypothesis.

In this study, 50% of the *Syngap1*^{+/-} mice presented with seizures during the 24-hour recording period, indicating a high incidence of seizures. Progressive worsening of sleep dysfunction and increasing NREM IIS frequency in 100% of the mice are also common features of several developmental disorders associated with epilepsy (53–59).

Wakefulness is associated with net-synaptic potentiation, whereas sleep favors global synaptic depression, thereby preserving an overall balance of synaptic strength (60). AMPAR levels are high during wakefulness and low during sleep. The global reduction of AMPARs during sleep may be disrupted in *Syngap1*^{+/-} mice because haploinsufficiency could result in the inability to regulate Ras and Rap, two proteins that are involved in the regulation of surface AMPARs (3,4,61–64). The inability to downregulate surface AMPARs during transition-state synaptic homeostasis could lead to chronic overexpression of AMPARs in highly active neurons, such as fast-spiking PV⁺ INs.

The significant loss in cortical gamma homeostasis associated with behavioral-state transitions in *Syngap1*^{+/-} mice

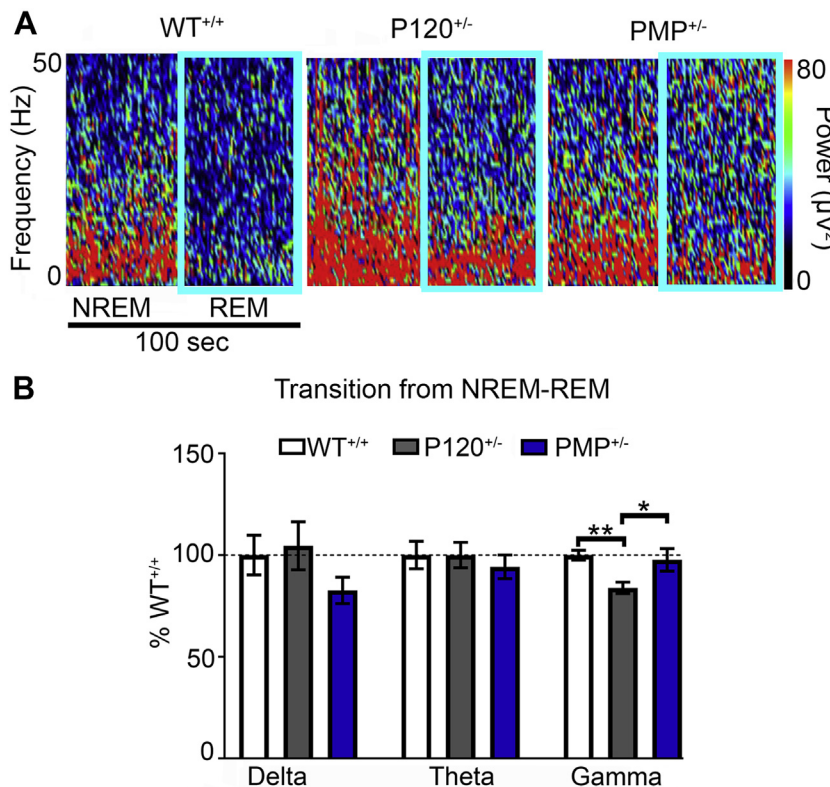


Figure 8. PMP rescued gamma modulation during transitions from NREM to REM. **(A)** Spectral power heat maps during NREM-to-REM transitions in WT^{+/+} mice, P120^{+/-} mice, and PMP^{+/-} mice. **(B)** A significant decrease in gamma power during NREM-to-REM transitions was demonstrated in P120^{+/-} mice (WT^{+/+} gamma % vs. P120^{+/-} gamma %: 1-way analysis of variance, $F_{2,105} = 6.11$, $p = .005$), but was significantly rescued by PMP administration (P120^{+/-} gamma % vs. PMP gamma %: 1-way analysis of variance, $F_{2,105} = 6.11$, $p = .026$). WT^{+/+} $n = 6$, P120^{+/-} $n = 7$, PMP^{+/-} $n = 4$. * $p < .05$, ** $p < .01$, post hoc Bonferroni corrections. NREM, non-rapid eye movement; P, postnatal day; P120^{+/-}, *Syngap1*^{+/-} mice at postnatal day 120; PMP, perampanel; PMP^{+/-}, PMP administered *Syngap1*^{+/-} mice; REM rapid eye movement; WT, wild-type.

could critically impede cortical information processing. Gamma oscillations (52,65) are known to depend on AMPAR kinetics in INs, especially for long-range synchrony. The significant rescue of the cortical gamma homeostasis by acute

dosing of low-dose PMP, compared with the relatively weaker effect on IIS suppression, may indicate a novel role for PMP beyond its Food and Drug Administration-approved antiseizure properties. New trials evaluating PMP efficacy in infants

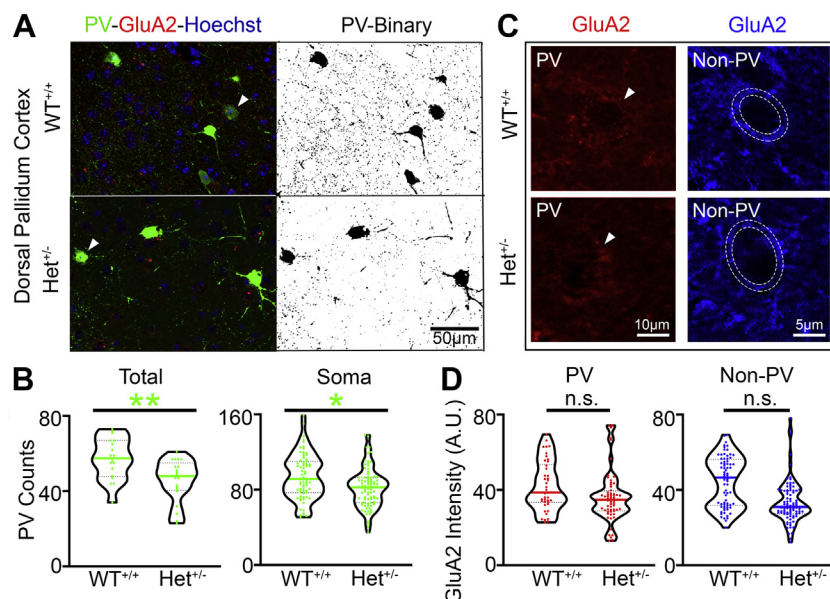


Figure 9. PV⁺ IN deficits in prefrontal cortex. **(A)** Representative $\times 40$ Z-stack image from the DP cortex in WT^{+/+} and *Syngap1*^{+/-} (Het^{+/-}) mice. White arrowheads indicate PV⁺ INs shown in **(C)**. **(B)** PV immunofluorescence represented by total PV⁺ puncta in the $\times 40$ image showed a significantly lower putative presynaptic puncta in the Het^{+/-} mice (nested t test, $t_{37} = 3.24$, $p = .0026$). PV⁺ puncta counts onto non-PV somas were also significantly lower (nested t test, $t_{14} = 2.398$, $p = .03$). **(C)** Representative images of GluA2 fluorescence on PV (red) and non-PV (blue) somas in the DP cortex in WT^{+/+} and Het^{+/-} mice. White arrowheads indicate soma of respective PV⁺ INs from **(A)**. **(D)** There were no significant differences in GluA2 expression on PV⁺ (nested t test, $t_{14} = 1.230$, $p = .2391$) or non-PV⁺ (nested t test, $t_{14} = 1.883$, $p = .0806$) INs in the DP cortex. Het^{+/-} $n = 8$, WT^{+/+} $n = 8$. * $p < .05$, ** $p < .01$. DP, dorsal pallidum; n.s., not significant; PV⁺ IN, parvalbumin-positive interneuron; WT, wild-type.

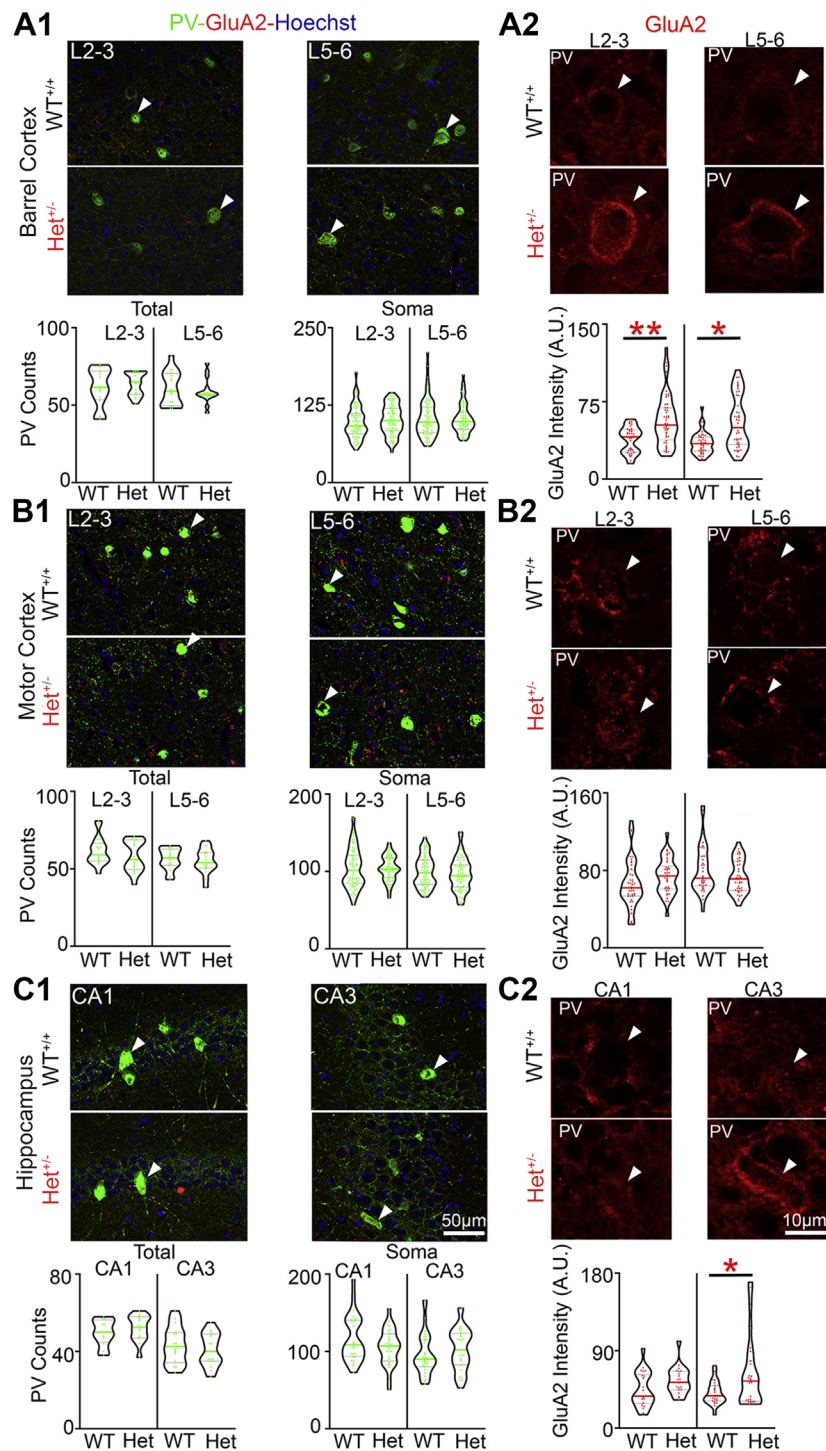


Figure 10. Increased GluA2 expression on PV⁺ INs were region specific. **(A1)** Representative $\times 40$ Z-stack images of WT^{+/+} and *Syngap1*^{+/-} (Het^{+/-}) mice from BCX layers 2–3 and 5–6. White arrowheads indicate PV⁺ INs shown in **(A2)**. Total PV⁺ puncta counts and somatic PV⁺ puncta counts on non-PV⁺ soma were not significantly different in the BCX. **(A2)** Representative Z-stack images of GluA2 immunofluorescence on PV⁺ INs in L2–3 and L5–6. Het^{+/-} GluA2 expression was significantly higher on PV⁺ INs in both BCX L2–3 (nested t test, $t_{12} = 3.467$, $p = .0047$) and L5–6 (nested t test, $t_{12} = 2.361$, $p = .036$). White arrowheads indicate soma of respective PV⁺ INs from **(A1)**. **(B1)** Representative $\times 40$ Z-stack images from MCX L2–3 and L5–6. Total PV⁺ puncta counts and somatic PV⁺ puncta counts on non-PV⁺ soma were not significantly different in the MCX. White arrowheads indicate PV⁺ INs shown in **(B2)** for MCX L2–3 and L5–6. **(B2)** Representative Z-stack images of GluA2 expression was not significantly different for PV⁺ INs in MCX L2–3 and L5–6. White arrowheads indicate soma of respective PV⁺ INs from **(B1)**. **(C1)** Representative $\times 40$ Z-stack images from hippocampal regions CA1 and CA3. White arrowheads indicate PV⁺ INs shown in **(C2)**. Total PV⁺ puncta counts and somatic PV⁺ puncta counts on non-PV⁺ soma were not significantly different in CA1 or CA3. **(C2)** Representative images of GluA2 immunofluorescence on PV⁺ INs. Het^{+/-} CA3 PV⁺ INs had a significant increase in GluA2 expression (nested t test, $t_{12} = 2.331$, $p = .038$). White arrowheads indicate soma of respective PV⁺ INs from **(C1)**. Het^{+/-} $n = 8$, WT^{+/+} $n = 8$. * $p < .05$, ** $p < .01$. A.U., arbitrary units; BCX, barrel cortex; L, layers; MCX, motor cortex; PV⁺ IN, parvalbumin-positive interneuron; WT, wild-type.

(23) are underway. In the clinic, PMP dosing is gradually ramped up, starting with the low dose of 2 mg/kg, in weekly increments, reaching maintenance doses of 8–12 mg/day based on tolerability. The acute low-dose protocol used here did not show significant effects on IIS suppression; however,

no seizure events were noted with PMP treatment. PMP anti-seizure efficacy for SYNGAP1-related seizures is currently unknown, and a recent cohort study with 57 patients reported only 1 patient that received PMP treatment (12). The findings indicate the necessity to develop GluA2-AMPAR-selective

antagonists, which currently do not exist. These analyses also identified poor PV⁺ IN innervation in the prefrontal cortex, which is supported by previously published reports (66) and was not detected in the other regions of interest.

Increasingly, brain oscillations are being used to understand complex neuropsychiatric disorders. Gamma oscillations (35–50 Hz) have warranted special attention owing to their association with higher-order cognitive processes, including sensory processing, attention, working memory, and executive functioning. Activation of GABAergic IN networks has been shown to produce gamma oscillations (~40 Hz) in both the hippocampal and neocortical networks. Given the critical role of PV⁺ INs in cortical gamma oscillations (48,67) and the role of AMPARs in homeostatic synaptic plasticity (68), the loss of gamma homeostasis identified for *Syngap1* haploinsufficiency during periods commonly associated with intense synaptic plasticity (69) provide novel insights into the associated intellectual disabilities. AMPA-mediated currents rise and decay faster in INs partly because of these differences in subunit profiles (70,71). PV⁺ INs receive convergent excitatory input from principal neurons and inhibitory input primarily from other PV⁺ INs. Experiments that have causally tested stimulation of PV⁺ cells *in vivo* in the BCX by ontogenetic manipulation selectively amplified gamma oscillations (72). Importantly, this activation suppressed the sensory processing in nearby excitatory neurons within the BCX. Findings of increased GluA2-AMPARs on PV⁺ soma both in layers 2–3 and in 5–6 of the BCX would predict similar suppression of sensory processing in the BCX (73). An increase of GluA2 expression in PV⁺ INs in the BCX could implicate recruitment of excessive PV⁺ IN-mediated inhibition resulting in cortical hyperexcitability via rebound excitation. This hypothesis may underlie the clinical reports of reflex seizures in MRD5 emerging during activities associated with increased cortical gamma synchronicity (12,31), a role in which electrically coupled projection PV⁺ INs are significantly involved.

The morphology of PV⁺ INs has been identified as unipolar versus multipolar (74), and little is known about the differences in AMPA-mediated currents in these subtypes. GluA2-lacking AMPARs promote anti-Hebbian long-term plasticity (75), which is critical for projection INs that functionally connect spatially distant circuits during development. Increase of GluA2-AMPARs in PV⁺ IN soma could be one novel mechanism underlying autistic-like behaviors, ID, and seizures in SYNGAP1 haploinsufficiency. Little is known of the developmental and regional expression profiles of SYNGAP1 isoforms, but it is known that they can exert opposing effects on synaptic strength (76).

In summary, SYNGAP1 regulates synaptic plasticity, and this process is heavily involved in both epileptogenesis and sleep homeostasis. Investigation of circuit function in intact brains using qEEG biomarkers during the transitions between active exploratory, inactive wake, and REM/NREM sleep states is an exciting frontier. These behavioral-state transitions are the most reliant on synaptic plasticity.

ACKNOWLEDGMENTS AND DISCLOSURES

Research reported in this publication was supported by the Eunice Kennedy Shriver National Institute of Child Health and Human Development of the

National Institutes of Health under Grant No. R01HD090884 (to SDK). The content is solely the responsibility of the authors and does not necessarily represent the official views of the National Institutes of Health.

We thank the families who consented to participate in the post hoc analyses of overnight EEGs recorded in their children with identified pathogenic SYNGAP1 mutations. We also thank the Bridge the Gap SYNGAP foundation for help with patient EEG acquisition. We thank Dr. Jonathan Pevsner for his thoughtful comments and suggestions and Dr. Ingie Hong for his help with the GluA2-knockout immunohistochemistry experiments.

This article was published as a preprint on bioRxiv: doi: <https://doi.org/10.1101/718965>.

The authors report no biomedical financial interests or potential conflicts of interest.

ARTICLE INFORMATION

From the Neuroscience Laboratory (BJS, PAK, SDK), Hugo Moser Research Institute, Kennedy Krieger Institute; Department of Neuroscience (YA, RLH), Kavli Neuroscience Discovery Institute, Johns Hopkins University School of Medicine, and Department of Neurology (SDK), Johns Hopkins University School of Medicine, Baltimore, Maryland; and Department of Neurological Surgery (SA), University of California San Francisco, San Francisco, California.

Address correspondence to Shilpa D. Kadam, Ph.D., Hugo Moser Research Institute, Kennedy Krieger Institute, 707 North Broadway, 400H, Baltimore, MD 21205; E-mail: kadam@kennedykrieger.org.

Received Aug 21, 2019; revised and accepted Dec 19, 2019.

Supplementary material cited in this article is available online at <https://doi.org/10.1016/j.biopsych.2019.12.025>.

REFERENCES

- Chen H-J, Rojas-Soto M, Oguni A, Kennedy MB (1998): A synaptic Ras-GTPase activating protein (p135 SynGAP) inhibited by CaM kinase II. *Neuron* 20:895–904.
- Kim JH, Liao D, Lau LF, Huganir RL (1998): SynGAP: A synaptic RasGAP that associates with the PSD-95/SAP90 protein family. *Neuron* 20:683–691.
- Rumbaugh G, Adams JP, Kim JH, Huganir RL (2006): SynGAP regulates synaptic strength and mitogen-activated protein kinases in cultured neurons. *Proc Natl Acad Sci U S A* 103:4344–4351.
- Araki Y, Zeng M, Zhang M, Huganir RL (2015): Rapid dispersion of SynGAP from synaptic spines triggers AMPA receptor insertion and spine enlargement during LTP. *Neuron* 85:173–189.
- Zeng M, Bai G, Zhang M (2019): Anchoring high concentrations of SynGAP at postsynaptic densities via liquid-liquid phase separation. *Small GTPases* 10:296–304.
- Purcell SM, Moran JL, Fromer M, Ruderfer D, Solovieff N, Roussos P, et al. (2014): A polygenic burden of rare disruptive mutations in schizophrenia. *Nature* 506:185–190.
- Hamdan FF, Gauthier J, Spiegelman D, Noreau A, Yang Y, Pellerin S, et al. (2009): Mutations in SYNGAP1 in autosomal nonsyndromic mental retardation. *N Engl J Med* 360:599–605.
- Hamdan FF, Daoud H, Piton A, Gauthier J, Dobrzeniecka S, Krebs M-O, et al. (2011): De novo SYNGAP1 mutations in nonsyndromic intellectual disability and autism. *Biol Psychiatry* 69:898–901.
- Berryer MH, Hamdan FF, Klitten LL, Möller RS, Carmant L, Schwartzentruber J, et al. (2012): Mutations in SYNGAP1 cause intellectual disability, autism, and a specific form of epilepsy by inducing haploinsufficiency. *Hum Mutat* 34:385–394.
- Carvill GL, Heavin SB, Yendle SC, McMahon JM, O'Roak BJ, Cook J, et al. (2013): Targeted resequencing in epileptic encephalopathies identifies de novo mutations in CHD2 and SYNGAP1. *Nat Genet* 45:825–830.
- Mignot C, Stülpnagel C von, Nava C, Ville D, Sanlaville D, Lesca G, et al. (2016): Genetic and neurodevelopmental spectrum of SYNGAP1-associated intellectual disability and epilepsy. *J Med Genet* 53:511–522.
- Vlaaskamp DRM, Shaw BJ, Burgess R, Mei D, Montomoli M, Xie H, et al. (2019): SYNGAP1 encephalopathy: A distinctive generalized

- developmental and epileptic encephalopathy. *Neurology* 92:e96–e107.
13. Jain SV, Kothare SV (2015): Sleep and epilepsy. *Semin Pediatr Neurol* 22:86–92.
 14. Robinson-Shelton A, Malow BA (2016): Sleep disturbances in neurodevelopmental disorders. *Curr Psychiatry Rep* 18:6.
 15. Malow BA (2004): Sleep disorders, epilepsy, and autism. *Ment Retard Dev Disabil Res Rev* 10:122–125.
 16. Glaze DG (2005): Neurophysiology of Rett syndrome. *J Child Neurol* 20:740–746.
 17. Amman S, Chan WC, Adler DA, Lakshamanan BM, Gupta SS, Ewen JB, et al. (2015): Heightened delta power during slow-wave-sleep in patients with Rett syndrome associated with poor sleep efficiency. *PLoS One* 10:e0138113.
 18. Johnston MV, Amman S, O'Driscoll C, Wozniak A, Naidu S, Kadam SD (2014): Twenty-four hour quantitative-EEG and in-vivo glutamate biosensor detects activity and circadian rhythm dependent biomarkers of pathogenesis in *Mecp2* null mice. *Front Syst Neurosci* 8:118.
 19. Holmes GL (2005): Effects of seizures on brain development: Lessons from the laboratory. *Pediatr Neurol* 33:1–11.
 20. Nabbot R, Dulac O (2003): Epileptic encephalopathies: A brief overview. *J Clin Neurophysiol* 20:393–397.
 21. Prchalova D, Havlovicova M, Sterbova K, Stranecky V, Hancarova M, Sedlacek Z (2017): Analysis of 31-year-old patient with SYNGAP1 gene defect points to importance of variants in broader splice regions and reveals developmental trajectory of SYNGAP1-associated phenotype: Case report. *BMC Med Genet* 18:62.
 22. Villanueva V, Montoya J, Castillo A, Mauri-Llerda JA, Giner P, López-González FJ, et al. (2018): Perampanel in routine clinical use in idiopathic generalized epilepsy: The 12-month GENERAL study. *Epilepsia* 59:1740–1752.
 23. Epilepsy Foundation: Perampanel Study for Infants With Epilepsy. Available at: https://www.epilepsy.com/clinical_trials/perampanel-study-infants-epilepsy. Accessed January 23, 2019.
 24. Clement JP, Ozkan ED, Aceti M, Miller CA, Rumbaugh G (2013): SYNGAP1 links the maturation rate of excitatory synapses to the duration of critical-period synaptic plasticity. *J Neurosci* 33:10447–10452.
 25. Clement JP, Aceti M, Creson TK, Ozkan ED, Shi Y, Reish NJ, et al. (2012): Pathogenic SYNGAP1 mutations impair cognitive development by disrupting maturation of dendritic spine synapses. *Cell* 151:709–723.
 26. Kim JH, Lee H-K, Takamiya K, Huganir RL (2003): The role of synaptic GTPase-activating protein in neuronal development and synaptic plasticity. *J Neurosci* 23:1119–1124.
 27. Kang SK, Amman S, Thodupunuri S, Adler DA, Johnston MV, Kadam SD (2018): Sleep dysfunction following neonatal ischemic seizures are differential by neonatal age of insult as determined by qEEG in a mouse model. *Neurobiol Dis* 116:1–12.
 28. Adler DA, Amman S, Lei J, Dada T, Borbely T, Johnston MV, et al. (2014): Circadian cycle-dependent EEG biomarkers of pathogenicity in adult mice following prenatal exposure to *in utero* inflammation. *Neuroscience* 275:305–313.
 29. Kennedy Krieger Institute, Johns Hopkins University School of Medicine (2018): Research study: Overnight EEGs from children with SYNGAP1 mutations needed for a research study (2018) Available at: https://www.kennedykrieger.org/sites/default/files/library/documents/research/participate-in-research/KADAM%20IRB_Flyer_V2%209%2018%202018%20approved.pdf. Accessed July 1, 2019.
 30. ImageJ: Image Processing and Analysis in Java () Available at: <https://imagej.nih.gov/ij/>. Accessed July 1, 2019.
 31. Striano P, Huppke P (2019): A synaptic protein defect associated with reflex seizure disorder. *Neurology* 92:63–64.
 32. Baud MO, Kleen JK, Mirro EA, Andrechak JC, King-Stephens D, Chang EF, Rao VR (2018): Multi-day rhythms modulate seizure risk in epilepsy. *Nat Commun* 9:88.
 33. Bains RS, Wells S, Sillito RR, Armstrong JD, Cater HL, Banks G, Nolan PM (2018): Assessing mouse behaviour throughout the light/dark cycle using automated in-cage analysis tools. *J Neurosci Methods* 300:37–47.
 34. Nakajima R, Takao K, Hattori S, Shoji H, Komiya NH, Grant SGN, Miyakawa T (2019): Comprehensive behavioral analysis of heterozygous *Syngap1* knockout mice. *Neuropsychopharmacol Rep* 39:223–237.
 35. Komiya NH, Watabe AM, Carlisle HJ, Porter K, Charlesworth P, Monti J, et al. (2002): SynGAP regulates ERK/MAPK signaling, synaptic plasticity, and learning in the complex with postsynaptic density 95 and NMDA receptor. *J Neurosci* 22:9721–9732.
 36. Belluscio MA, Mizuseki K, Schmidt R, Kemper R, Buzsáki G (2012): Cross-frequency phase-phase coupling between θ and γ oscillations in the hippocampus. *J Neurosci* 32:423–435.
 37. Buzsáki G, Anastassiou CA, Koch C (2012): The origin of extracellular fields and currents—EEG, ECoG, LFP and spikes. *Nat Rev Neurosci* 13:407–420.
 38. Bragin A, Jandó G, Nádasdy Z, Hetke J, Wise K, Buzsáki G (1995): Gamma (40–100 Hz) oscillation in the hippocampus of the behaving rat. *J Neurosci* 15:47–60.
 39. Soltesz I, Deschénes M (1993): Low- and high-frequency membrane potential oscillations during theta activity in CA1 and CA3 pyramidal neurons of the rat hippocampus under ketamine-xylazine anesthesia. *J Neurophysiol* 70:97–116.
 40. Axmacher N, Henseler MM, Jensen O, Weinreich I, Elger CE, Fell J (2010): Cross-frequency coupling supports multi-item working memory in the human hippocampus. *Proc Natl Acad Sci U S A* 107:3228–3233.
 41. Demiralp T, Bayraktaroglu Z, Lenz D, Junge S, Busch NA, Maess B, et al. (2007): Gamma amplitudes are coupled to theta phase in human EEG during visual perception. *Int J Psychophysiol* 64:24–30.
 42. Köster M, Friese U, Schöne B, Trujillo-Barreto N, Gruber T (2014): Theta-gamma coupling during episodic retrieval in the human EEG. *Brain Res* 1577:57–68.
 43. Lisman JE, Jensen O (2013): The theta-gamma neural code. *Neuron* 77:1002–1016.
 44. Moretti DV, Fracassi C, Pievani M, Geroldi C, Binetti G, Zanetti O, et al. (2009): Increase of theta/gamma ratio is associated with memory impairment. *Clin Neurophysiol* 120:295–303.
 45. Buzsaki G, Wang XJ (2012): Mechanisms of gamma oscillations. *Annu Neurosci* 35:203–225.
 46. Valderrama M, Crépon B, Botella-Soler V, Martinerie J, Hasboun D, Alvarado-Rojas C, et al. (2012): Human gamma oscillations during slow wave sleep. *PLoS One* 7:e33477.
 47. Scheffzük C, Kukushka VI, Vyssotski AL, Draguhn A, Tort ABL, Brankačk J (2011): Selective coupling between theta phase and neocortical fast gamma oscillations during REM-sleep in mice. *PLoS One* 6:e28489.
 48. Sohal VS, Zhang F, Yizhar O, Deisseroth K (2009): Parvalbumin neurons and gamma rhythms enhance cortical circuit performance. *Nature* 459:698–702.
 49. Tremblay R, Lee S, Rudy B (2016): GABAergic interneurons in the neocortex: From cellular properties to circuits. *Neuron* 91:260–292.
 50. Huang ZJ, Paul A (2019): The diversity of GABAergic neurons and neural communication elements. *Nat Rev Neurosci* 20:563–572.
 51. Akgül G, McBain CJ (2016): Diverse roles for ionotropic glutamate receptors on inhibitory interneurons in developing and adult brain. *J Physiol* 594:5471–5490.
 52. Fuchs EC, Doheny H, Faulkner H, Caputi A, Traub RD, Bibbig A, et al. (2001): Genetically altered AMPA-type glutamate receptor kinetics in interneurons disrupt long-range synchrony of gamma oscillation. *Proc Natl Acad Sci U S A* 98:3571–3576.
 53. Xu L, Guo D, Liu Y-Y, Qiao D-D, Ye J-Y, Xue R (2018): Juvenile myoclonic epilepsy and sleep. *Epilepsy Behav* 80:326–330.
 54. Gruber R, Wise MS (2016): Sleep spindle characteristics in children with neurodevelopmental disorders and their relation to cognition. *Neural Plast* 2016:4724792.
 55. Singh NS, Sullivan JE (2014): Continuous spike-wave during slow wave sleep and related conditions. *ISRN Neurol* 2014:619079.

56. Al Keilani MAH, Carlier S, Groswasser J, Dan B, Deconinck N (2011): Rett syndrome associated with continuous spikes and waves during sleep. *Acta Neurol Belg* 111:328–332.
57. Creson TK, Rojas C, Hwaun E, Vaissiere T, Kilinc M, Jimenez-Gomez A, et al. (2019): Re-expression of SynGAP protein in adulthood improves translatable measures of brain function and behavior. *eLife* 8:e46752.
58. Ozkan ED, Creson TK, Kramár EA, Rojas C, Seese RR, Babyan AH, et al. (2014): Reduced cognition in *Syngap1* mutants is caused by isolated damage within developing forebrain excitatory neurons. *Neuron* 82:1317–1333.
59. Ujma PP, Simor P, Ferri R, Fabó D, Kelemen A, Erőss L, et al. (2015): Increased interictal spike activity associated with transient slow wave trains during nonrapid eye movement sleep. *Sleep Biol Rhythms* 13:155–162.
60. Vyazovskiy VV, Cirelli C, Pfister-Genskow M, Faraguna U, Tononi G (2008): Molecular and electrophysiological evidence for net synaptic potentiation in wake and depression in sleep. *Nat Neurosci* 11:200–208.
61. Zhu JJ, Qin Y, Zhao M, Van Aelst L, Malinow R (2002): Ras and Rap control AMPA receptor trafficking during synaptic plasticity. *Cell* 110:443–455.
62. Walkup WG, Washburn L, Swerdford MJ, Carlisle HJ, Graham RL, Hess S, Kennedy MB (2015): Phosphorylation of synaptic GTPase-activating protein (synGAP) by Ca^{2+} /calmodulin-dependent protein kinase II (CaMKII) and cyclin-dependent kinase 5 (CDK5) alters the ratio of its GAP activity toward Ras and Rap GTPases. *J Biol Chem* 290:4908–4927.
63. Krapivinsky G, Medina I, Krapivinsky L, Gapon S, Clapham DE (2004): SynGAP-MUPP1-CaMKII synaptic complexes regulate p38 MAP kinase activity and NMDA receptor-dependent synaptic AMPA receptor potentiation. *Neuron* 43:563–574.
64. Pena V, Hothorn M, Eberth A, Kaschau N, Parret A, Gremer L, et al. (2008): The C2 domain of SynGAP is essential for stimulation of the Rap GTPase reaction. *EMBO Rep* 9:350–355.
65. Fuchs EC, Zivkovic AR, Cunningham MO, Middleton S, LeBeau FEN, Bannerman DM, et al. (2007): Recruitment of parvalbumin-positive interneurons determines hippocampal function and associated behavior. *Neuron* 53:591–604.
66. Berryer MH, Chattopadhyaya B, Xing P, Riebe I, Bosoi C, Sanon N, et al. (2016): Decrease of SYNGAP1 in GABAergic cells impairs inhibitory synapse connectivity, synaptic inhibition and cognitive function. *Nat Commun* 7:13340.
67. Le Magueresse C, Monyer H (2013): GABAergic interneurons shape the functional maturation of the cortex. *Neuron* 77:388–405.
68. Altimimi HF, Stellwagen D (2013): Persistent synaptic scaling independent of AMPA receptor subunit composition. *J Neurosci* 33:11763–11767.
69. Turrigiano G (2011): Too many cooks? Intrinsic and synaptic homeostatic mechanisms in cortical circuit refinement. *Annu Rev Neurosci* 34:89–103.
70. Jonas P (1994): Differences in Ca^{2+} permeability of AMPA-type glutamate receptor channels in neocortical neurons caused by differential GluR-B subunit expression. *Neuron* 12:1281–1289.
71. Hu H, Gan J, Jonas P (2014): Fast-spiking, parvalbumin⁺ GABAergic interneurons: From cellular design to microcircuit function. *Science* 345(6196):1255263.
72. Cardin JA, Carlén M, Meletis K, Knoblich U, Zhang F, Deisseroth K, et al. (2009): Driving fast-spiking cells induces gamma rhythm and controls sensory responses. *Nature* 459:663–667.
73. Michaelson SD, Ozkan ED, Aceti M, Maity S, Llamosas N, Weldon M, et al. (2018): SYNGAP1 heterozygosity disrupts sensory processing by reducing touch-related activity within somatosensory cortex circuits. *Nat Neurosci* 21:1–13.
74. Blatow M, Rozov A, Katona I, Hormuzdi SG, Meyer AH, Whittington MA, et al. (2003): A novel network of multipolar bursting interneurons generates theta frequency oscillations in neocortex. *Neuron* 38:805–817.
75. Kullmann DM, Lamsa K (2008): Roles of distinct glutamate receptors in induction of anti-Hebbian long-term potentiation. *J Physiol* 586:1481–1486.
76. McMahon AC, Barnett MW, O'Leary TS, Stoney PN, Collins MO, Papadia S, et al. (2012): SynGAP isoforms exert opposing effects on synaptic strength. *Nat Commun* 3:900.